Catena 196 (2021) 104932

Contents lists available at ScienceDirect

Catena

journal homepage: www.elsevier.com/locate/catena

Advancements and challenges in rill formation, morphology, measurement and modeling

Xiaojing Ou[a,d], Yaxian Hu[a,b,d,*], Xianwen Li[c], Shengli Guo[b,d], Baoyuan Liu[b,d]

[a] State Key Laboratory of Soil Erosion and Dryland Farming on the Loess Plateau, Institute of Soil and Water Conservation, Chinese Academy of Sciences and Ministry of Water Resources, Yangling, Shaanxi 712100, China
[b] Institute of Soil and Water Conservation, Northwest A&F University, Yangling, Shaanxi 712100, China
[c] Key Laboratory of Agricultural Soil and Water Engineering in Arid and Semiarid Areas, Ministry of Education, Northwest A&F University, Yangling, Shaanxi 712100, China
[d] University of Chinese Academy of Sciences, Beijing 100049, China

ARTICLE INFO

Keywords:
Rill erosion process
Rill morphology
Rill measurement
Rill flow
Rill modeling

ABSTRACT

Rill erosion is a small-scale but universally occurring phenomenon. Given its potential to concentrate into larger-scale erosion and its non-negligible contributions to soil loss, substantial research has been dedicated to understanding its processes. In this article, we conducted a holistic review of the major achievements in rill erosion research over the past few decades, mainly from the following perspectives: 1) Hydraulic parameters to describe rill development; 2) morphological indicators to represent rill morphology; 3) commonly used measuring methods for rill morphology and rill flow; and 4) advantages and limitations of rill erosion modelling. In each of the perspectives, we also identified the challenges faced by current rill erosion research. Concrete suggestions on the pressing needs to help advance rill erosion research in the future are further presented.

1. Introduction

Rills are defined as small intermittent watercourses with steep sides that are initiated due to differential erosion caused by overland flow (Zheng and Gao, 2003). They often have a width and depth of 2–20 cm (Liu et al., 2018). Rill erosion is the process of dispersing, scouring, and transportation of soil during rill formation and development (Zheng and Gao, 2003). It extensively occurs in human-disturbed areas (Fig. 1) (Govers et al., 2007; Guo et al., 2019), especially in sloping farmland, where rill-induced soil loss accounts for 50–70% of the total soil erosion (He et al., 2014). Due to the small dimensions of the rills, the soil transported in rills is generally composed of fine particles (Luk et al., 1993) and has the potential to selectively deplete nutrients and fertility from agricultural land (Aksoy et al., 2020). Progressively, multiple adjacent rills can combine to form an ephemeral gully with a wider shallow groove that can further facilitate flow convergence. Further, an ephemeral gully may evolve into a gully if the downcutting depth exceeds the ploughing depth (Fig. 2). When this occurs, the gap of a gully cannot be re-filled by farming practices (Stefano et al., 2013); this eventually leads to severe land degradation (Daba et al., 2003; Valentin et al., 2005). Therefore, it is essential to quantitatively understand rill erosion processes, so that soil and nutrient deterioration can be prevented at the primary stage before soil degradation becomes irreversible.

The detachment of soil particles and the development of rills are governed by soil properties and flow hydraulic characteristics (Nearing et al., 1991). Once a rill is formed, the sediment concentrations in it will increase rapidly, promptly changing rill morphology and, in turn, altering the hydraulic properties and soil loss (Nearing et al., 1997; Lei et al., 1998; Gatto, 2000). In addition, sediment transport in the rill flow is strongly influenced by the inter-rill flow input from the upslope (Luk et al., 1993). Detached particles may also enter the rill via raindrop impact (Kinnell, 2001), change rill flow energy, and consequently alter the way the rill is shaped. Timely capture of the ever-changing and interactive rill processes in the field and quantitative determination of hydrodynamics during rill erosion is difficult; hence, most previous research on rill erosion has been conducted under controlled conditions in the laboratory (Shen et al., 2016; X. Zhang et al., 2018; Aksoy et al., 2020). It has primarily focussed on the hydrodynamics of rill erosion, quantitative parameters of rill morphology, and rill erosion modelling under controlled conditions (Govindaraju and Kavvas, 1992; Lu et al., 2003; Govers et al., 2007; Wagenbrenner et al., 2010; Han et al., 2011; Wirtz et al., 2012; Tian et al., 2017; Ran et al., 2018; Mirzaee et al., 2020). However, rills are far more complex under natural conditions

* Corresponding author at: Xinong Road 26, Yangling 712100, China.
E-mail address: huyaxian@nwafu.edu.cn (Y. Hu).

https://doi.org/10.1016/j.catena.2020.104932
Received 24 February 2020; Received in revised form 18 September 2020; Accepted 21 September 2020
Available online 01 October 2020
0341-8162/ © 2020 Elsevier B.V. All rights reserved.

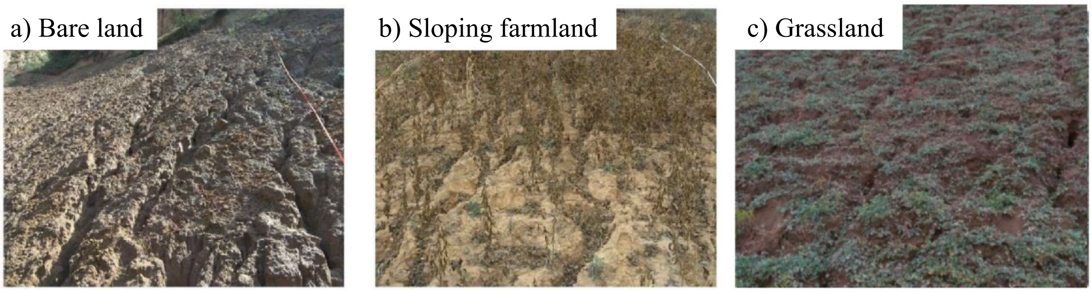

Fig. 1. Rills on different land use types (Guo et al., 2019).

Fig. 2. Erosional ditches of different scales (Liu et al., 2018).

than those studied under specific controlled conditions (often a single or a certain number of rills generated by predetermined rainfall events on selected slope gradients), and the adequate and efficient adaptation of the conclusions drawn from these controlled experiments to the real eroding field remains unclear. Hence, this article reviews the current achievements in rill erosion research both under laboratory conditions and in the field, identifying the most relevant knowledge gaps and pressing challenges with an overview of the potential solutions that can be implemented in the future.

2. Rill initiation and development

2.1. Factors influencing rill initiation and development

The initiation of a rill depends on both soil resistance and flow hydraulic characteristics. Theoretically, a rill starts when the shear force of flow on the slope exceeds soil resistance (Merz and Bryan, 1993; Knapen and Poesen, 2009). As to the pattern of rill initiation and development, a well-accepted theory is that due to the heterogeneity of the soil surface, runoff is very likely to converge at certain positions and then scour out a knickpoint (Slattery and Bryan, 1992; Owoputi and Stolte, 1995) (Fig. 3), denoting the initial state of a rill (He et al., 2013).

Fig. 3. Typical scoured knickpoint (Merz and Bryan, 1993).

Thereafter, overland flow continues to concentrate and grow more erosive to expand the knickpoint. Over a period of continuous scouring, knickpoints on the same flow path converge into a connected rill, aggravating soil erosion.

Based on the above-described theory, we recognise that rill initiation and development processes are influenced by both internal and external factors. Internal factors mainly refer to soil physicochemical properties that define soil erodibility, such as soil bulk density, composition of soil particles and aggregates, and organic matter content. For instance, soils with heavy density are capable of repressing rill erosion as a result of strong interlock forces being formed among the soil particles (Hieke and Schmidt, 2013). Compacted or clay-rich soils often require higher erosive forces to be eroded, and thus are less likely to form rills (Rauws and Auzet, 1989; Govers et al., 1990; Yanosek et al., 2006; Chen et al., 2015). In addition, organic matter plays an important role in binding aggregates; soils rich in organic matter can withstand destruction such as slaking or micro-fissuration when raindrop impact or rapid wetting occurs (Tisdall and Oades, 1982; Govers et al., 1990). Meanwhile, macro-aggregates with abundant pore spaces enable more infiltration and thus help retard rill erosion (Hieke and Schmidt, 2013). Hence, soils of lower density and more stable aggregate structures are less susceptible to rill erosion (Govers, 1991; Barthès and Roose, 2002). All these inherent soil properties can directly or indirectly affect sub-processes such as infiltration, aggregate breakdown, and sediment detachment (Sheridan et al., 2000), and consequently, influence rill erosion.

External factors affecting rill erosion mainly include slope gradient, slope aspect, slope length, land use, surface roughness, and vegetation coverage (Smith and Wischmeier, 1957; Römkens et al., 2002). By comparing six barren spoil heaps, Beullens et al. (2014) found that the dominant southwest wind brought more rainfall and thus resulted in greater rill erosion on the southwestern than on the western facing slopes. The experiments with run-on on undisturbed soil conducted by Li et al. (2015) indicated that land use affects soil properties and vegetation (and hence, root characteristics), and therefore, could significantly affect rill erodibility. Zhao et al. (2017) reported that compared to a smooth slope, contour tillage (with ridges and furrows) helped to reduce soil loss by 30–60% during rill erosion, while reservoir tillage (with depressions and mounds) increased rill erosion by 25%. In addition to individual impacts, these external factors can also interact

Table 1
Hydraulic parameters widely used to investigate rill erosion.

Parameter	Equation	Description	Reference
Mean flow velocity	$V = \alpha V_s$	V is mean flow velocity (m s^{-1}); α is correction factor; V_s is surface flow velocity (m s^{-1}).	Abrahams et al., 1986
Froude number	$Fr = \frac{V}{\sqrt{gh}}$	Fr is Froude number; g is gravitational acceleration (m s^{-2}); h is rill flow depth (m).	Chow, 1959
Reynolds number	$Re = \frac{VR}{\upsilon}$	Re is Reynolds number; R is hydraulic radius; υ is viscosity coefficient of rill flow (m^2 s^{-1}).	Chow, 1959
Shear stress	$\tau = \rho ghS$	τ is shear stress (Pa); ρ is water mass density (kg m^{-3}); S is the sine value of slope gradients.	Nearing et al., 1991
Shear velocity	$u_* = \sqrt{gRS}$	$u_*$is shear velocity (cm s^{-1}).	Govers, 1985
Stream power	$\omega = \rho ghSV = \tau V$	ω is stream power (W m^{-2}).	Bagnold, 1966
Unit stream power	$U = VS$	U is unit stream power (m s^{-1}).	Yang, 1972

with each other to alter soil properties and regulate changes in hydraulic conditions during rill initiation and development.

2.2. Rainfall simulations and field investigations to define hydraulic parameters during rill processes

In theory, soil detachment and transport during rill erosion are mainly governed by concentrated rill flow and are thus closely related to hydraulic parameters (Table 1) (Huang et al., 1996; Kinnell, 2006; Wang et al., 2016). Given the difficulties in capturing the drastic changes of rill erosion processes in the field, laboratory simulations with manageable and repeatable conditions have become a widely employed method to investigate hydraulic conditions during rill erosion processes (Hamed et al., 2002). For a certain soil type, some researchers described the hydraulic threshold of rill initiation as a constant but others consider that it varies within a certain range. For example, Govers (1985) determined the critical shear velocity for rill occurrence on loamy soils as 3.0–3.5 cm·s^{-1} and Merz and Bryan (1993) observed that the critical shear velocity was 5–6.5 cm·s^{-1} for sandy loam soils. However, Yao et al. (2008) reported that the critical mean flow velocity ranged from 3.2 to 5.2 cm·s^{-1} for loess (silty clay) soil, while the critical shear stress varied between 1.33 and 2.63. Furthermore, as rill performance differs among different soils (Slattery and Bryan, 1992), some studies have attempted to relate the hydraulic threshold of rill initiation to soil properties. For instance, Cai (1998) carried out a field experiment on loess soil with simulated rainfall and employed stream power as the indicator for rill generation:

$$E_{wr} = 1.27 + 0.28K_\tau \quad (1)$$

where E_{wr} is the critical stream power (W·m^{-2}) and K_τ is the antecedent soil shear strength (kPa). Eq. (1) provides a simple and practical way to determine the threshold of rill initiation for loess soils, as the shear strength can be measured easily in the field using a torsional vane before a rainfall event. Rauws and Govers (1988) concluded that effective shear velocity could be directly related to rill formation, and pointed out that the regression equation (Eq. (2)) could be used for rill prediction for a wide range of soils under field conditions:

$$u_{gcr} = 0.89 + 0.56C \quad (2)$$

where u_{gcr} is the critical effective shear velocity (cm·s^{-1}) and C is the apparent cohesion of the topsoil (kPa). A much more thorough investigation was conducted by Gilley et al. (1993), wherein a broad range of soil samples was collected and selective properties, such as soil particle distribution, water-dispersible clay content, soil water content, coefficient of linear extensibility, and cation exchange capacity, were quantified in detail. For each soil, a rill was generated in the field with five flow discharges. After obtaining the critical value for each soil, a multiple regression was applied to relate them to selected soil properties, where critical shear stress was significantly correlated to water-dispersible clay. Hence, they proposed that for soils with water-dispersible clay content less than 7.5%, the correlation can be expressed as follows:

$$\tau_c = 0.216(clay) - 183(coefficient\ of\ linear\ extensibility) + 0.412(soil\ water\ content\ at\ 1.5MPa) + 0.78 \quad (3)$$

where clay and soil water content at 1.5 MPa are given as percentages and the coefficient of linear extensibility is in cm/cm. For soils with a water-dispersible clay content of 7.5% or greater, the correlation between critical shear stress and water-dispersible clay can be expressed as follows:

$$\tau_c = 0.296(calcium) + 1.53(iron) + 7.75(organic\ carbon) - 11.4(potassium) - 0.535(very\ fine\ sand) - 0.208 \quad (4)$$

where calcium and potassium content are in cM/kg, and iron, organic carbon, and very fine sand are given as percentages.

Despite extensive studies on hydraulic thresholds for rill initiation on different soils, it remains difficult to generalise a universally applicable equation to describe the variations in rill initiation. In most cases, only basic soil properties, such as particle distribution, were presented; however, soil erodibility is affected by a variety of physical, chemical, and biological characteristics. Further, the definition and descriptions of rill initiation are not consistent among different reports. For example, Torri et al. (1987) considered a rill to be initiated when its incision was 5 cm long, 1–2 cm wide, and 0.5 cm deep, while others reported only a qualitative description, such as "a small pit that develops into rill" (Yao et al., 2008). An even more commonly used approach to determine rill incision is to detect an increase in sediment yield. As reported by Rauws and Govers (1988), a rill is initiated when a small channel is deep enough to concentrate the flow at least a few decimetres long along the flow path, causing a detectable increase in sediment discharge. Zhang and Yasuhiro (1998), by analysing the relationship between sediment discharge and erosion depth, defined such erosion as a rill if it had a depth of more than 0.8–1 cm. Overall, previous studies have clearly demonstrated that rill initiation is very soil specific, which is decisively but not exclusively, influenced by primary soil properties, such as soil particle distribution, clay types and contents, and precedent soil moisture. However, equations or hydraulic thresholds established on single or selective soil properties under specific experimental conditions can only partially represent the complex development of rill erosion. Incompatible experimental designs in different reports and the authors' biasness in describing the key results make it more difficult to effectively compare and then generalise a widely applicable theory on rill initiation and hydraulic thresholds. Standard protocols with well-defined boundary conditions are urgently required to develop a sound and comprehensive approach to advance our current understanding of rill initiation.

As for rill development, because the hydraulic forces inducing sediment detachment may not be responsible for sediment transport (Giménez and Govers, 2002), different experiments are often required to identify the controlling hydraulic variables for sediment detachment and transport. Among a variety of parameters, stream power, unit stream power, and shear stress are the most widely adopted indicators. However, depending on the soil type and experimental set-up, such as slope gradients, inflow discharges, treatments of soils (natural or

Table 2
Most widely used rill morphology parameters.

Parameters	Notion	Equation	Description	Reference
Rill density	Total length of rill per unit land area	$\rho = \sum_{j=1}^{n} L_{tj}/A_0$	ρ is rill density (m m^{-2}); L_{tj} is the total length of the *j*-th rill and its branches (m); A_0 is the land area (m^2).	Bewket and Sterk, 2003
Degree of rill dissection	Plane areas of all rills per unit land area	$\mu = \frac{\sum_{j=1}^{n} A_j}{A_0}$	μ is the degree of rill dissection; A_j is area of the *j*-th rill (m^2).	Shen et al., 2015
Rill width-depth ratio	Ratio of rill width to corresponding depth	$R_{WD} = \frac{\sum_{i=1}^{n} W_i}{\sum_{i=1}^{n} D_I}$	R_{WD} is the ratio of rill width to corresponding depth; W_i is the rill width of location *i* (cm); D_i is the rill depth of location *i* (cm).	He et al., 2013
Rill complexity	The ratio of the total length of a rill and its branches on the slope to the vertical length in the slope direction	$c = \frac{L_{tj}}{L_j}$	*c* is rill complexity; L_{tj} is the total length of the *j*-th rill and its branches (m); L_j is the vertical length of the *j*-th rill (m).	Shen et al., 2015
Fractal dimension	A parameter for quantitative expression of fractal complexity	$N = Cr^{-D_f}$	D_f is the fractal dimension; *C* is a constant value; *r* is the rectangular side length covering the slope (mm); *N* is the number of objects related to *r*.	Foroutan-pour et al., 1999
Geomorphic information entropy	A concept from analogy of entropy in thermodynamics to geomorphology	$H = S - \ln S - 1$	*H* is geomorphic information entropy; *S* is Strahler area-elevation integral value.	Ai, 1987

disturbed), and bed surface conditions (flat or irregular), the optimal indicator for rill erosion may vary from one experiment to another. For example, Wang et al. (2019) reported that when considering varying sediment loads in rill flow, stream power performed better in predicting the soil detachment rate than shear stress and unit stream power. Niu et al. (2020) also observed that flow shear stress was poorly related to soil detachment rate with a low correlation coefficient of 0.48. However, Giménez and Govers (2002) pointed out that shear stress could be related to rill detachment without being affected by bed geometry, while the prediction by stream power or unit stream power was dependent on bed geometry. Regarding the transport capacity of overland flow, investigations are often conducted on non-erodible beds (soil beds are glued to maintain constant roughness throughout experiments) while being fed with a flow of varying sediment loads until maximum transport capacity is reached. Following this protocol, Zhang et al. (2009) suggested that shear stress could be applied to predict transport capacity on steep slopes. Wu et al. (2016) also proposed that shear stress and stream power are efficient parameters in simulating rill flow transport capacity for steep loess slopes. Nevertheless, conclusions are drawn differently when employing erodible beds; Moore and Burch (1986) and Finkner et al. (1989) preferred the simplicity and robustness of the transport equation by applying unit stream power as the driving force. Ali et al. (2012) conducted flume experiments with four well-sorted sands and proposed that unit stream power was the optimal flow force to predict transport capacity, as shear stress did not perform well due to partial dissipation of energy by sediment detachment and bed roughness.

Despite these achievements in describing rill development based on selective parameters, soil erosion rates vary over time and at different rill positions and thus should not be calculated using one equation but by integrating various spatiotemporal erosion processes (Wirtz et al., 2013). Polyakov and Nearing (2003) pointed out that during different stages of rill erosion, the equilibrium sediment loads are different, which means that the transport capacity is not constant even under the same experimental set-up and hydraulic conditions. Hence, spatio-temporally varying sub-processes such as rill head advancement and sidewall expansion should be separately accounted for (Qin et al., 2019a, 2019b). A typical limitation of the indoor experiments is that the conclusions drawn from them are only applicable to specific conditions under which the experiments have been conducted; these are often not verified or further generalised and thus cannot be directly applied to detect critical conditions for rill initiation or assess rill erosion intensity in the field. As an example, Shainberg et al. (1994) discovered that the critical shear stress was considerably lower in laboratory experiments than that determined in the field. Gilley et al. (1993) also mentioned that equations established in a field study where the residue was removed and newly tilled should not be applied to other areas with different soil or vegetation characteristics. Hence, hydraulic parameters determined by indoor simulation studies should not be directly applied to field conditions without appropriate verification or amendments (Zhang et al., 2003).

3. Rill morphology and its quantitative parameters

To unravel the relationship between rill morphology and rill erosion loss, it is necessary to develop parameters that can quantitatively characterise the complexity, irregularity, and multidimensionality of rill morphology (Zhang et al., 2019). Primary parameters to describe the morphology of a single rill include rill length, width, depth, and cross-sectional area as well as some statistical average values, such as average rill width and depth (Cerdan et al., 2002; Bewket and Sterk, 2003; Bruno et al., 2008; Qin et al., 2018; Ran et al., 2018). Based on several experiments, it has been found that these parameters are good indicators of rill processes as they are highly correlated or functionally linked with sediment load or rill erosion rate (Bruno et al., 2008; Shen et al., 2015; Chen et al., 2016).

After a rill is formed, it will continue to erode the headward and pass-side slope flow path, causing a local dint and consequently, a high flow concentration; this is when a tributary rill begins to form (Brunton and Bryan, 2000). Individual rills further bifurcate, merge, or connect to each other, resulting in a complex rill network system (Shen et al., 2014). The rill network is the initial and a miniature form of the drainage system through which sediment is transported from land to the river courses (Zhang et al., 2014), especially in arid areas and agricultural land (Brunton and Bryan, 2000). Over the past several decades, studies have introduced many parameters, such as rill density, degree of dissection, and complexity, to quantitatively describe rill networks (Table 2) (Bewket and Sterk, 2003; Berger et al., 2010; Zhang and Yang, 2010; Zhang et al., 2014; Zhang et al., 2016). Zhang et al. (2016) reported that fractal geometry could effectively reflect the complexity of the rill network on flumes filled with loess soil but failed to represent erosion intensity, especially when the rill network evolved to a stable state. Meanwhile, geomorphologic comentropy was capable of reflecting dynamic changes in rill erosion because it varied sensitively as rill erosion proceeded. Moreover, the principle of energy consumption has also been regarded as a reliable indicator for rill network development in laboratory studies. According to this theory, the rill network develops in the direction that causes the lowest energy consumption (Berger et al., 2010):

$$E = k\sum_{i=1}^{i=n} L_i A_i^{0.5} = minimum \tag{5}$$

where E is the sum of the energy of each rill link (W·m^{-2}), k is a constant depending on the soil fluid properties, L_i is the length of rill link i, and A_i is the contribution area for rill link i. In agreement with Eq. (5), Gómez et al. (2003), after carrying out a simulated rainfall experiment with varied slope gradients (5% and 20%) and soil roughness degrees (low, moderate, and great), reported that when rills were intense, the rill network evolution followed the principle of energy consumption. Furthermore, Rieke-Zapp and Nearing (2005) also observed that energy consumption was a quantifiable indicator of rill network development based on a test with five different slope shapes (uniform, concave-linear, convex-linear, nose slope, and head slope).

It is noteworthy that most of the above-summarised equations or theories implicitly assumed that rill morphology is homogeneous and stable. Rill morphology and sediment discharge may change greatly over time at different stages during the rill erosion process (Xiao et al., 2008; Jiang et al., 2018; Niu et al., 2020). C. Qin et al. (2019a, 2019b) outlined rill development as follows: 1) Rill head advancement at the early stage, 2) bed incision until the soil layer becomes less erodible, and 3) sidewall expansion caused by rill toe scouring. They further explored the proportions of sediment yield induced by the three sub-processes and found that head advancement made a major contribution to rill erosion (44%–68%), followed by bed incision (27%–44%), and sidewall expansion (3.8%–12%). Therefore, the evolution of rill morphology has a strong heterogeneity, as the dominant erosion patterns are highly variable during an erosion event, contributing differently to total soil loss. Parameters derived from a stable rill morphology are not capable of distinguishing spatially specific morphological changes at different positions along a rill.

To better understand the features of rill morphology, previous investigations have attempted to relate soil properties to rill morphology. For example, Chen et al. (2013) found that the rills formed on the soil with higher clay content (28.42%) were denser and more parallel to each other, while the rills formed on the soil with lower clay content (14.52%) were dendritic with shorter and wider cross-sections. Zhao and Gao (2016), after summarising field survey data, concluded that rill width-depth ratios tended to decrease when the soil texture was finer. Ni et al. (2018) further confirmed that the prediction accuracy for soil erosion improved after including soil properties and rill morphology parameters.

To further explore the potential influences of other major variables (e.g., clay content, rainfall intensity, run-on scouring rate, and slope gradient) on rill morphology, we collated and compared the rill width-depth ratios generated from different rainfall and run-on simulation experiments (Fig. 4) (source data and literature are listed in Supplement 1). Soils with greater clay content appeared to form narrower and deeper rills under the same manner of erosive force (rainfall only or flow only) (Fig. 4a). Rill width-depth ratios tended to slightly decrease with rainfall intensity, regardless of run-on scouring effects (Fig. 4b). However, rills generated by run-on scouring seemed to be affected by erosive rainfall and were likely to become wider and shallower when run-on rates are greater (Fig. 4c). As for the potential influences of slope gradients on rill morphology, rills appeared to be narrower and deeper on steeper slopes (Fig. 4d).

Although Fig. 4 helps improve our current understanding of rill morphology, we must acknowledge several potential biases in our observations: 1) Given the limited availability of data on the targeted issue, coupling effects of different variables are not discussed here. 2) As rainfall or run-on experiments were carried out by certain research groups or focussed on specific regions, the selected soil types are not adequately representative to formulate generalisable conclusions. 3) To ensure the generation of detectable rills within a reasonably short period, the rainfall intensity in almost all the simulation experiments (> 50 mm h^{-1}) was set to be much greater than what is typically observed during actual rainfall events; slope gradients were often very steep (mostly are 20–40°). On the one hand, such preferential settings partly explain the noticeably greater rill width-depth ratios by run-on experiments (slope gradient $< 15°$) than by rainfall simulation experiments (Fig. 4d). On the other hand, to ensure that presumed rills would occur, the possible influences of different soil properties (e.g., soil texture, precedent moisture) on rill initiation and morphology are conveniently neglected in such experiments. Therefore, we are still far from elucidating the variations and patterns of rill morphology. How and to what extent can the results from the controlled experiments be incorporated to adequately reflect the real-world rill morphology still remain as imposing challenges in rill erosion research.

4. Measurement of rill morphology

Commonly used techniques to sketch a rill include contact-type tools, satellite-dependent tools, and digital photogrammetry methods (Table 3). Conventionally, rills are mapped by laying a ruler or profilometer at specific points of a rill (Fig. 5); recording the width, depth, and cross-sections; and then sketching the rill morphology (Casalí et al., 2006; Kimaro et al., 2008). In this way, each rill section is usually assumed to be a rectangle for convenience (Peng et al., 2015). Together with the potential human error in misreading the metre, rill morphology sketched in this conventional manner is often of very limited accuracy (Vinci et al., 2016). Owing to advances in technology, digital techniques have been introduced to map rills. For instance, a laser scanner can identify rill boundaries and extract other fundamental morphological information (e.g., length, width, depth) by precisely determining the positions of abundant point clouds from different angles and distances (Vinci et al., 2015). However, point clouds acquired from multi-station scanning are often of heterogeneous densities, and thus are very labour-intensive to process (Zhang et al., 2011). The high cost of a laser scanner also hinders its wide application (Zhang et al., 2008).

Compared to laser scanning, photogrammetry is much less expensive and capable of acquiring images with an even higher resolution (Guo et al., 2016; Jiang et al., 2020). Recent studies have demonstrated that close-range photogrammetry can efficiently capture micro-morphological changes during erosion processes and produce digital elevation models (DEMs) with millimetre-scale resolution (Balaguer-Puig et al., 2017; Campbell et al., 2018). Furthermore, photogrammetry can detect soil surface changes even during rain, enabling the continuous tracking of the evolvement of rill morphology (Jiang et al., 2020).

Unmanned aerial vehicles (UAVs) have also been proven to be a very practical tool to assist soil erosion research. By stitching the highly overlapping images taken by the UAV, a precise DEM can be generated to analyse the micro-topographic changes on eroding landforms. A few studies have employed UAVs to investigate soil erosion at various scales from rill erosion at plot-scale, gullies on slopes, and sediment transport in watersheds (Liu et al., 2016; Feng and Li, 2018; Krenz and Kuhn, 2018; C. Yang et al., 2018). It was proved that when flying at a low altitude (e.g., 50 or 100 m), the ground sampling distance of UAV images can reach 4 cm or even 2 cm (C. Zhang et al., 2018), especially if the ground control points are strictly calibrated by a high-precision satellite positioning system (e.g., real-time kinematic positioning). If the UAV flight altitude is further reduced to 10 or 20 m, the ground sampling distance of UAV images can reach the millimetre scale, which is more than adequate to map small-scale erosion (Anguiano-Morales et al., 2018), such as rills with sizes of 2–20 cm. In addition, unlike laser scanning and photogrammetry, UAVs have the advantage of easily covering a watershed within a relatively short time and flexibly adjusting the flight altitude to meet the requirements of different spatial resolutions. Nevertheless, the potential of applying UAVs to study soil erosion, especially small-scale rill erosion, is far from being fully explored. Standard protocols with specific descriptions of flight routes, set-up of ground control points, and image processing are pressingly needed. The rapid development of drones and easy accessibility of high-resolution cameras promises great opportunities for better utilisation of UAVs to investigate rill erosion in the future.

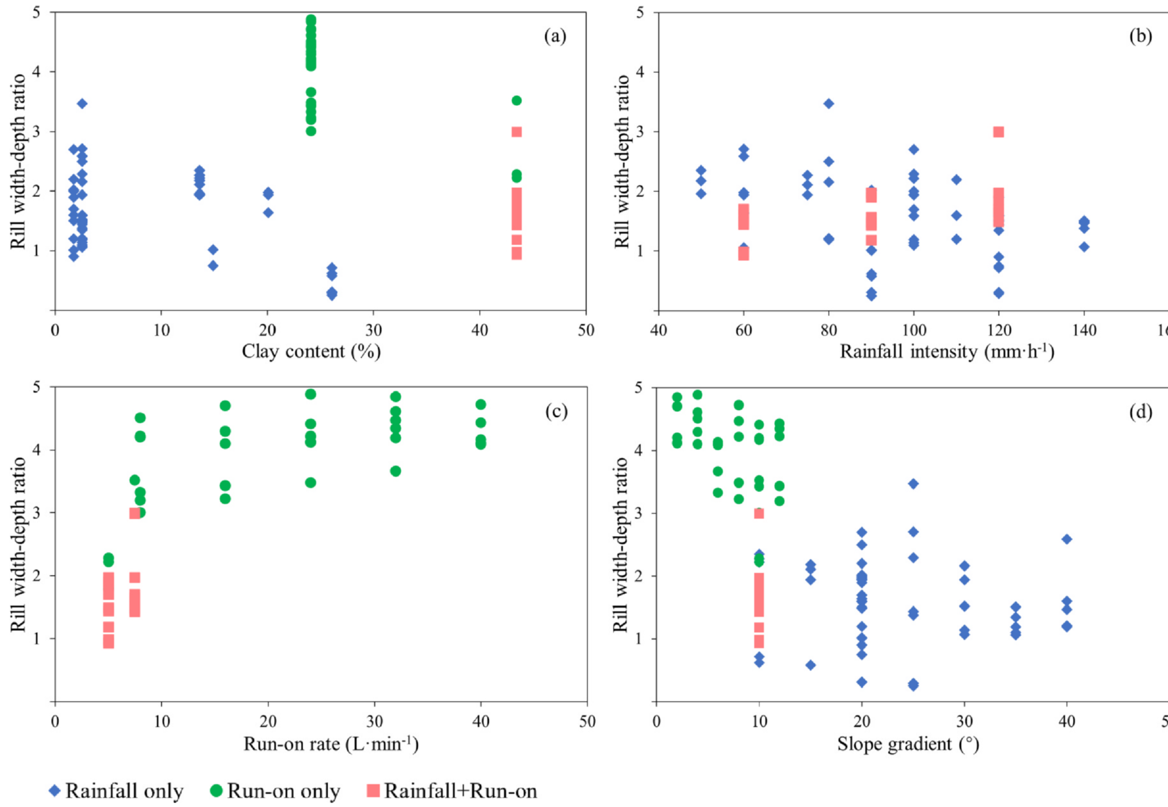

Fig. 4. Changes in rill width-depth ratio under different clay contents, rainfall intensities, run-on rates, and slope gradients based on previous reports.

Table 3
Most widely used tools for measuring rill morphology.

Tool	Advantages	Limitations	References
Tape/Ruler	Costs low and straightforward to operate	1) Difficult and time-consuming to measure cross-sections; 2) results tend to bear large errors	Casalí et al., 2006; Castillo et al., 2012
Profiles	Able to precisely delimit rill cross-sections	1) Requiring great field labor even in small areas; 2) difficult to reproduce measurements	Wells et al., 2016;Casalí et al., 2006; Jester and Klik, 2005
Total station	Capable of high temporal resolutions by user-defined revisit cycles	1) Discrete data requiring interpolation processing susceptible to unknown uncertainty; 2) not available in areas with poor satellite coverage	Wells et al., 2016; Westoby et al., 2012
GPS	1) Quick and easy to operate; 2) fairly robust even in unfavorable weather	Not available in areas with poor satellite coverage	Brasington et al., 2015; Westoby et al., 2012
TLS	1) High-precision data available; 2) redundant objects like vegetations automatically filtered	1) Large incidence angle may reduce sampling density; 2) costly and not portable	Vinci et al., 2015; Wells et al., 2016; Westoby et al., 2012
Photogrammetry	1) Images with high resolution of centimeter to millimeter scale; 2) time- and labor-efficient	1) Time consuming and requiring professional pre-knowledge; 2) merely plausible for small plots or laboratories	Eltner et al., 2015; Jester and Klik, 2005; Qin et al., 2019a, 2019b; Wells et al., 2016
UAV	1) Portable and possible to be equipped with various sensors to fulfill different expectations; 2) flight to be planned in advance to realize semi-automatic data acquisition	Relying heavily on weather (e.g., often hindered by high-speed wind)	Eltner et al., 2015; Westoby et al., 2012

5. Measurement of rill flow

To quantitatively measure rill flow and calculate hydraulic parameters, some elementary rill flow features, such as flow width, depth, and average flow velocity, must be acquired first. Nevertheless, unstable rill flow velocity, irregular rill surfaces, and high sediment concentrations make it exceedingly difficult to measure the relevant hydraulic parameters of rill flow (Govers, 1992; Qin et al., 2016).

The most convenient way to measure rill flow width and depth is to use ruler tape, callipers, or water level metres (Gong et al., 2008). Although easy to operate, they cannot acquire high-resolution records as they are very prone to be biased by the interference of turbulent rill flow or subject to potential human error in misreading the metre. Newly advanced techniques, such as laser scanning and close-range photogrammetry, enable scanning or taking snapshots of rills at predetermined time intervals, effectively capturing rill flow features with high spatial–temporal resolutions (Vinci et al., 2015). However, given the ever-changing rill bed, it is still excessively challenging to measure rill flow features in time, especially when raindrops and turbulent flow interfere during rainfall events.

The dye-tracer technique has been widely adopted to measure rill flow velocity owing to its low cost and simplicity (Fig. 6a) (Peng et al.,

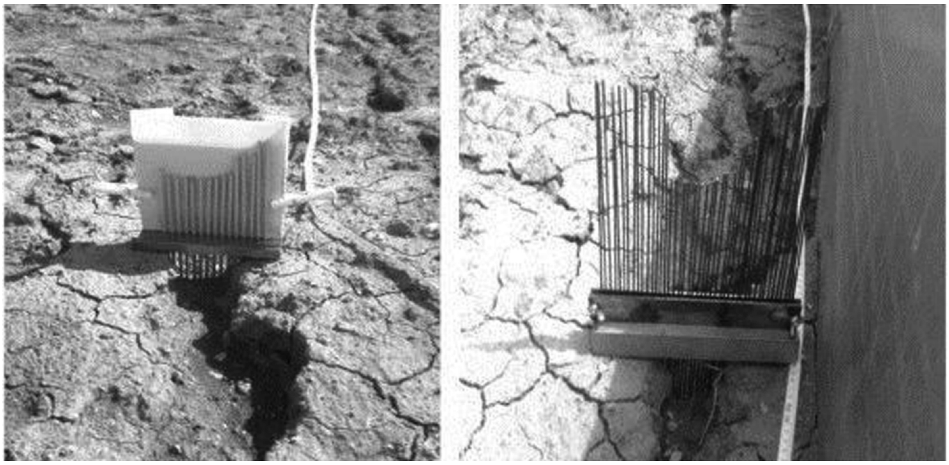

Fig. 5. Profilometers used to manually measure rills (Vinci et al., 2015).

2015). By adding dye to water, the dye speed can be calculated by the time it takes to travel from the injection point over a known distance, the result of which is often assumed to represent the flow velocity at the fluid surface. After calibration, the average velocity of the rill flow can be obtained. However, there has been no universally accepted coefficient to convert surface flow velocity into the average velocity of the rill flow (Zhang et al., 2010). In addition, dye-tracing requires an adequately long distance to travel, which would otherwise introduce misinterpretation by dye diffusion or the dye might be discharged too rapidly out of the plot to record the travelling time (Dong et al., 2014).

Apart from dye-tracing, other materials such as salt solution, fluorescent particles, or light-density floats have also been employed as tracers in different studies (Liu et al., 2007; Tauro et al., 2010; Zhuang et al., 2018). For instance, the salt-tracing technique uses the differences in electrical conductivity to distinguish between the travelling time, and thereby, the flow velocities of the salted and non-salted waters (Fig. 6b). After detecting the conductivity of the salted water in the rill flow, the sensor will transfer the timing signals to the recorder and document them on the computer. However, during rill erosion processes in the field, soil may absorb or dissolve the salt that has been artificially added to the rill flow, and infiltration may also percolate the salt out of the rill flow, jointly leading to biased estimation. In recent years, optical velocity methods, such as particle image velocimetry and particle tracking velocimetry, have been developed to estimate flow surface velocity using digital cameras or lasers to track the motion of particles dispersed in a fluid (e.g., fluorescent particles or air bubbles) (Coz et al., 2010; Tauro et al., 2016). Nevertheless, they are normally used in large-scale surveys such as rivers or oceans, where the flow is adequately deep and not turbulent. An infra-red sensor (or infra-red camera) can also be used to estimate the velocity of the shallow flow by detecting the movement of a thermal tracer in a fluid (e.g., warmer water or ice cubes) (Lima et al., 2015). Similar to dye-tracing methods, the thermal tracing technique estimates the flow velocity by dividing the travelling distance by the time required by the tracer to travel between the injection and the measuring points (Abrantes et al., 2018). Compared with other visible tracers, thermal signals are easier to capture in images; thermal imaging can also perform well in darkness (Mujtaba and Lima, 2018; Abrantes et al., 2019). However, thermal equipment is often costly (Abrantes et al., 2019). Overall, more accurate, adaptable, user-friendly, and less costly techniques are urgently needed to capture the spatiotemporal variability of rill flow velocity.

6. Rill erosion modelling

Rill erosion modelling is a fundamental part of slope-scale erosion prediction, providing a theoretical basis and references for soil erosion investigation and erosion risk assessment. Some commonly used models for rill prediction are listed in Table 4. Most of the currently available soil erosion models have been developed to estimate soil loss amount and formulate conservation measures. Hence, the spatiotemporal variations in small-scale erosion, such as rill erosion, are often simplified in these models (Lei et al., 1998). For instance, in the well-known Water Erosion Prediction Project (WEPP), many simplified assumptions have been adopted when modelling rill erosion. However, some of them do not conform to the real conditions in the field; for example, 1) the cross-sections of a rill are all assumed to be rectangular and the distance between two adjacent rills is set as 1 m in the WEPP (Mancilla et al., 2005); 2) the hydraulic characteristics of all rills are assumed to be similar (Favis-Mortlock et al., 2000); 3) rill width is only functionally related to the discharge and rill erosion does not interact with rill morphology; and 4) critical shear stress is set as constant when rills are formed (Nouwakpo et al., 2010). Furthermore, the actual runoff values are unknown and have to be predicted, which can be difficult (Kinnell, 2016). All such assumptions and deficiencies need to be corrected or improved when attempting rill erosion modelling with more reasonable predictions.

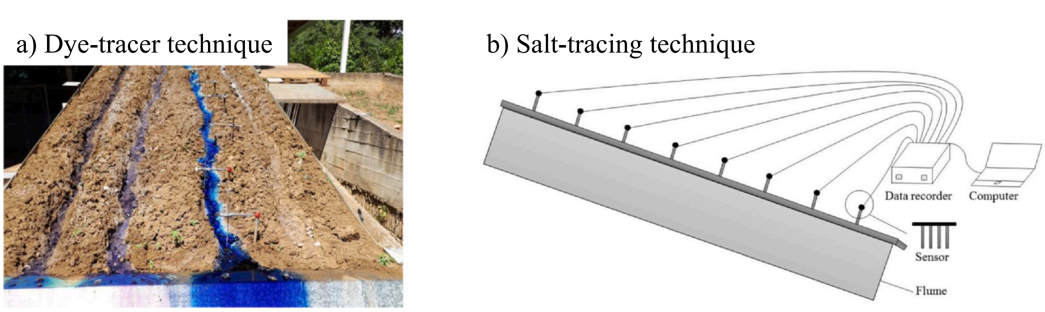

Fig. 6. Techniques for measuring rill flow velocity (Stefano et al., 2020).

Table 4
Comparisons of the most widely applied models for rill erosion prediction.

Model	Hypothesis	Advantages	Limitations	References
WEPP	1) The main erosive force in a rill is rill flow; 2) net detachment in rills occurs when flow shear stress exceeds soil critical shear strength and sediment load is less than transport capacity; 3) net deposition occurs when sediment load is greater than transport capacity.	1) WEPP is capable of predicting soil loss or gain on a hillslope (or each unit in it) on a daily, monthly, or average annual basis; 2) process-based algorithm allows it to be applied to various condition.	During a storm, it simulates only total soil loss with assumed steady flow, which cannot reflect how sediment discharge varies over time.	Morgan et al., 1998; Nearing et al., 1989
RillGrow	Rills are self-organized systems	Input required by the model is just detailed data of micro-topography.	Requirements on abundant data and mass computation do not favor it to be applied to large areas such as a watershed or even a field.	Favis-Mortlock et al., 2000; Zheng et al., 2004
GUEST	In a rill, entrainment and re-entrainment by rill flow along with simultaneous deposition are the main processes controlling sediment concentration.	GUEST is able to distinct soil re-detachment and re-entrainment.	Rainfall and runoff erosion processes are separately determined and simply summed up without considering their interactions.	Chen et al., 2007; Mahmoodabadi et al., 2014; Misra and Rose, 1996
EUROSEM	1) Both splash and flow erosion occur in a rill; 2) Interrill areas incline towards rills rather than straight downslope; 3) erosion expands and deepens rills while deposition reduces rill depth.	1) EUROSEM takes changes in rill morphology into consideration; 2) able to simulate soil detachment, transport and deposition in a rill during individual storms; 3) not only predicts total soil loss but also generates dynamic sediment graph; 4) can be applied to both rilled and flat soil surface.	The maximum number of channels and planes is 60 (PC version), and thus they need to be integrated to be applied for large or complicated catchments. If increasing the input capacity, the catchment representation will become complex and data entry will be time-consuming.	De ROO et al., 1996; Morgan et al., 1998

Elliot and Laflen (1993) developed a rill erosion model using a series of equations based on the principles of soil mechanics, fluid mechanics, and soil physics. In this model, soil properties affecting soil erodibility were adequately considered, such as moisture content, soil texture, and aggregate stability. In addition, rill erosion is comprised of four different sub-processes in this model: scouring, headcutting, side sloughing, and dispersion. Both detachment and transport processes were estimated using different equations. Although largely improved compared to other models, their model assumed that rills were pre-existing and therefore it cannot be applied to predict where rills would occur.

Favis-Mortlock et al. (2000) developed a model named "RillGrow" to forecast the location and evolution of rills based on self-organising work systems. RillGrow is capable of reproducing reliable erosional networks after inputting microtopography data. Despite the evident advantages of being simple to apply, according to its creators, RillGrow also has some drawbacks: 1) Some important processes such as infiltration and deposition were ignored; 2) because of the high demands for computer performance, the size of the study area is largely constrained; and 3) the model requires very detailed microtopography data, which greatly limits its application. Lei et al. (1998) observed that rills are prone to form a self-distributing system with alternating detachment and deposition areas. In other words, great spatiotemporal variations may inevitably exist even under the most strictly controlled experimental conditions. Such inter-replicate discrepancies are not only introduced by soil heterogeneity, but also by the random distribution of rill flow and erosion area.

In addition to the universally applicable models mentioned above, some relatively simple rill models were also established for specific needs. For instance, Mancilla et al. (2005) developed an empirical model to predict rill density under four cultivation modes. It was based on variables such as rill flow rate, stubble coverage ratio, soil surface random roughness, precedent soil moisture, soil bulk density, and slope gradient. Although this model cannot be generalised to other scenarios where other factors are also at work, all the variables are easy to obtain and thus can provide a practical approach to help predict rill erosion under local conditions. Moreover, several models have been aiming to ascertain one or selected sub-processes in rill erosion, such as soil detachment (Wang et al., 2016; Mirzaee and Ghorbani-Dashtaki, 2018; Li et al., 2019), soil transport (Tayfur, 2007; Yan et al., 2008; Wu et al., 2016), sediment concentration in rill flow (D. Yang et al., 2018), erosion accelerated by gravity (Han et al., 2011), head advancing rate caused by bed incision (Qin et al., 2018), amongst others. One can easily refer to and adopt these models if he/she is interested in certain sub-processes.

Rill simulation can also become biased due to inadequate or inappropriate accounts of rill hydraulic characteristics, sediment movement, rill morphology, or rill flow parameters. For example, after theoretically analysing the relationship between rill length and sediment discharge, (Yao et al., 2004) pointed out that rill erodibility estimated by WEPP may have a high relative error of 50–90%, due to the difficulty in determining flow shear stress and sediment detachment. Zheng et al. (2020) found that the annual average soil loss simulated by WEPP tended to respond over-sensitively to the increase in slope gradient and slope length when slopes were steep and bare. They attributed the mis-estimation to the constant rill spacing of 1 m set as the default in WEPP. Furthermore, Zhang et al. (2019) observed that including rill morphology factors can improve the prediction accuracy of the soil erosion model proposed by Jiang et al. (1996), which can be used to predict soil erosion loss from steep slopes on the Chinese Loess Plateau. Consequently, the development of process-based rill erosion models requires detailed knowledge of the characteristics and hydrodynamics of rill flow, mechanisms of moving soil particles, and the evolving processes of rill morphology.

Moreover, it is essential to sub-divide rill erosion processes to separately identify the driving factors. For instance, soil erodibility not only varies in space but also changes over time during an erosion event (Kinnell, 2009). Accurate measurements of the relevant parameters (e.g., flow velocity and depth, rill morphology, and sediment yield) are also critical to laying the fundamental framework for rill erosion modelling. Given these inherent uncertainties and dynamics during rill initiation and development, currently available rill erosion models are far from sophisticated in reconstructing an evolving rill (Liu and An, 2007). The gaps between the theoretical models and actual situations are large and currently, are difficult to bridge. However, rill erosion models are of great value to help address soil erosion and its consequences in local regions. A reasonable rill evaluation index system and standard protocols to effectively evaluate and compare rill characteristics in different regions and scenarios are needed.

7. Summary and outlook

This article reviews the advancements in rill erosion over the past few decades and highlights the non-negligible role of small-scale rill erosion in soil loss. After identifying the critical conditions for rill initiation and the hydraulic parameters for rill development, this review summarises the uncertainties and challenges to quantitatively characterise rill morphology and rill flow features. This leads to a discussion on the development and limitations of the currently available rill erosion modelling. To address these challenging issues, this article calls for more focussed investigations in the future from the following perspectives:

1). Observations on rill initiation and development are often case-specific for certain soil types or slope conditions. However, potential influences of soil properties on soil erodibility and rill formation or morphology are often ignored while those of rainfall intensity or steep slope are overvalued. Field investigations on a wider range of soil types or indoor experiments under more realistic rainfall and slope conditions are necessary to practically evaluate and compare rill characteristics among different regions or scenarios.
2). Rill erosion features attained from a single or a certain number of rills cannot represent the complex evolvement of rills in the field. This largely hinders the design of rill-controlling measures to effectively prevent rills from developing into ephemeral or permanent gullies. Systematic investigations on rill network dynamics are therefore pressingly needed to advance our current understanding on the evolution of rills that ultimately cause soil degradation events on large scales.
3). Currently available rill erosion models are not able to effectively reconstruct a dynamically evolving rill. Apart from parameterising soil properties and slope conditions, these models also require the sub-division of rill erosion processes to separately identify driving factors for individual sub-processes and, more importantly, to systematically integrate these sub-processes to improve the plausibility and validity of rill erosion models in predicting soil loss at different rill positions at different stages.

Declaration of Competing Interest

The authors declare that they have no known competing financial interests or personal relationships that could have appeared to influence the work reported in this paper.

Acknowledgement

The research was supported by the National Key Research and Development Project of China (2018YFC0507001) and the National Natural Sciences Foundation of China (41701318, 41502225). The leading author are also grateful to Prof. Nikolaus J. Kuhn for his inspiration to encourage me to pursue research on rill erosion. We sincerely appreciate the reviewers and editor for the constructive comments on earlier versions of this manuscript.

Appendix A. Supplementary data

Supplementary data to this article can be found online at https://doi.org/10.1016/j.catena.2020.104932.

References

Abrahams, A.D., Parsons, A.J., Luk, S.-H., 1986. Field measurement of the velocity of overland flow using dye tracing. Earth Surf. Process. Landf. 11, 653–657. https://doi.org/10.1002/esp.3290110608.

Abrantes, J.R.C.B., Moruzzi, R.B., Lima, J.L.M.P.D., Silveira, A., Montenegro, A.A.A., 2019. Combining a thermal tracer with a transport model to estimate shallow flow velocities. Phys. Chem. Earth, Parts A/B/C 109, 59–69. https://doi.org/10.1016/j.pce.2018.12.005.

Abrantes, J.R.C.B., Moruzzi, R.B., Silveira, A., Lima, J.L.M.P.D., 2018. Comparison of thermal, salt and dye tracing to estimate shallow flow velocities: Novel triple-tracer approach. J. Hydrol. 557, 362–377. https://doi.org/10.1016/j.jhydrol.2017.12.048.

Ai, L.S., 1987. Comentropy in Erosional Drainage-System. J. Soil Water Conserv. 1, 3–10 (In Chinese).

Aksoy, H., Gedikli, A., Yilmaz, M., Eris, E., Unal, N., Yoon, J., Kavvas, M., Tayfur, G., 2020. Soil erosion model tested on experimental data of a laboratory flume with a pre-existing rill. J. Hydrol. 581, 5609–5624. https://doi.org/10.1016/j.jhydrol.2019.124391.

Ali, M., Sterk, G., Seeger, M., Boersema, M., Peters, P., 2012. Effect of hydraulic parameters on sediment transport capacity in overland flow over erodible beds. Hydrol. Earth Syst. Sci. 16, 591–601. https://doi.org/10.5194/hess-16-591-2012.

Anguiano-Morales, M., Corral-Martínez, L.F., Trujillo-Schiaffino, G., Salas-Peimbert, D.P., García-Guevara, A.E., 2018. Topographic investigation from a low altitude unmanned aerial vehicle. Opt. Lasers. Eng. 110, 63–71. https://doi.org/10.1016/j.optlaseng.2018.05.015.

Bagnold, R.A., 1966. An Approach to the Sediment Transport Problem From General Physics. USGPO, Washington.

Balaguer-Puig, M., Marqués-Mateu, Á., Lerma, J.L., Ibáñez-Asensio, S., 2017. Estimation of small-scale soil erosion in laboratory experiments with Structure from Motion photogrammetry. Geomorphology 295, 285–296. https://doi.org/10.1016/j.geomorph.2017.04.035.

Barthès, B., Roose, E., 2002. Aggregate stability as an indicator of soil susceptibility to runoff and erosion; validation at several levels. CATENA 47, 133–149. https://doi.org/10.1016/S0341-8162(01)00180-1.

Berger, C., Schulze, M., Rieke-Zapp, D., Schlunegger, F., 2010. Rill development and soil erosion: a laboratory study of slope and rainfall intensity. Earth Surf. Process. Landf. 35, 1456–1467. https://doi.org/10.1002/esp.1989.

Beullens, J., Van de Velde, D., Nyssen, J., 2014. Impact of slope aspect on hydrological rainfall and on the magnitude of rill erosion in Belgium and northern France. CATENA 114, 129–139. https://doi.org/10.1016/j.catena.2013.10.016.

Bewket, W., Sterk, G., 2003. Assessment of soil erosion in cultivated fields using a survey methodology for rills in the Chemoga watershed. Ethiopia. Agric. Ecosyst. Environ. 97, 81–93. https://doi.org/10.1016/S0167-8809(03)00127-0.

Brasington, J., Rumsby, B.T., Mcvey, R.A., 2015. Monitoring and modelling morphological change in a braided gravel-bed river using high-resolution GPS-based survey. Earth Surf. Process. Landf. 25, 973–990. https://doi.org/10.1002/1096-9837(200008)25:9<973::aid-esp111>3.0.co;2-y.

Bruno, C., Stefano, C.D., Ferro, V., 2008. Field investigation on rilling in the experimental Sparacia area. South Italy. Earth Surf. Process. Landf. 33, 263–279. https://doi.org/10.1002/esp.1544.

Brunton, D.A., Bryan, R.B., 2000. Rill network development and sediment budgets. Earth Surf. Process. Landf. 25, 783–800. https://doi.org/10.1002/1096-9837(200007)25:7<783::AID-ESP106>3.0.CO;2-W.

Cai, Q.G., 1998. Research of rill initiation condition on loess hillslopes. J. Sediment Res., 52–59. http://doi.org/10.16239/j.cnki.0468-155x.1998.01.006. (In Chinese).

Campbell, S., Simmons, R., Rickson, J., Waine, T., Simms, D., 2018. Using Near-Surface Photogrammetry Assessment of Surface Roughness (NSPAS) to assess the effectiveness of erosion control treatments applied to slope forming materials from a mine site in West Africa. Geomorphology 322, 188–195. https://doi.org/10.1016/j.geomorph.2018.08.027.

Casalí, J., Loizu, J., Campo, M.A., De Santisteban, L.M., Álvarez-Mozos, J., 2006. Accuracy of methods for field assessment of rill and ephemeral gully erosion. CATENA 67, 128–138. https://doi.org/10.1016/j.catena.2006.03.005.

Castillo, C., Pérez, R., James, M.R., Quinton, J.N., Taguas, E.V., Gómez, J.A., 2012. Comparing the Accuracy of Several Field Methods for Measuring Gully Erosion. Soil Sci. Soc. Am. J. 76, 1319–1332. https://doi.org/10.2136/sssaj2011.0390.

Cerdan, O., Bissonnais, Y.L., Couturier, A., Bourennane, H., Souchère, V., 2002. Rill erosion on cultivated hillslopes during two extreme rainfall events in Normandy. France. Soil Tillage Res. 67, 99–108. https://doi.org/10.1016/S0167-1987(02)00045-4.

Chen, J.J., Sun, L.Y., Cai, C.F., Liu, J.T., Cai, Q.G., 2013. Rill Erosion on Different Soil Slopes and Their Affecting Factors. Acta Pedol. Sin. 50, 281–288. http://doi.org/10.11766/trxb201204150134. (In Chinese).

Chen, X.Y., Huang, Y.H., Zhao, Y., Mo, B., Mi, H.X., 2015. Comparison of loess and purple rill erosions measured with volume replacement method. J. Hydrol. 530, 476–483.

https://doi.org/10.1016/j.jhydrol.2015.10.001.

Chen, X.Y., Zhao, Y., Mi, H.X., Mo, B., 2016. Estimating rill erosion process from eroded morphology in flume experiments by volume replacement method. CATENA 136, 135–140. https://doi.org/10.1016/j.catena.2015.01.013.

Chen, Y. H., Xie, C.B., Gan, P., Yu, Q.Y., Yu, X.X., 2007. Review on the present status of sediment yield due to soil erosion in watersheds. J. Sediment Res., 75–82. http://doi.org/10.16239/j.cnki.0468-155x.2007.03.014. (In Chinese).

Chow, T., 1959. Open-Channel Hydraulics. McGraw-Hill.

Coz, J.L., Hauet, A., Pierrefeu, G., Dramais, G., Camenen, B., 2010. Performance of image-based velocimetry (LSPIV) applied to flash-flood discharge measurements in Mediterranean rivers. J. Hydrol. 394, 42–52. https://doi.org/10.1016/j.jhydrol.2010.05.049.

Daba, S., Rieger, W., Strauss, P., 2003. Assessment of gully erosion in Eastern Ethiopia using photogrammetric techniques. CATENA 50, 273–291. https://doi.org/10.1016/S0341-8162(02)00135-2.

De ROO, A.P.J., Wesseling, C.G., Ritsema, C.J., 1996. LISEM: A Single-event Physically Based Hydrological and Soil Erosion Model for Drainage Basins. I: Theory, Input And Output. Hydrol. Process. 10, 1107–1117. http://doi.org/10.1002/(sici)1099-1085(199608)10:8 < 1107::Aid-hyp415 > 3.0.Co;2-4.

Dong, Y., Zhuang, X., Lei, T., Yin, Z., Ma, Y., 2014. A method for measuring erosive flow velocity with simulated rill. Geoderma 232, 556–562. https://doi.org/10.1016/j.geoderma.2014.06.014.

Elliot, W., Laflen, J., 1993. A Process-based Rill Erosion Model. Trans. ASAE 36, 65–72. https://doi.org/10.13031/2013.28315.

Eltner, A., Baumgart, P., Maas, H.-G., Faust, D., 2015. Multi-temporal UAV data for automatic measurement of rill and interrill erosion on loess soil. Earth Surf. Process. Landf. 40, 741–755. https://doi.org/10.1002/esp.3673.

Favis-Mortlock, D.T., Boardman, J., Parsons, A.J., Lascelles, B., 2000. Emergence and erosion: A model for rill initiation and development. Hydrol. Process. 14, 2173–2205. https://doi.org/10.1002/1099-1085(20000815/30)14:11/12 < 2173::AID-HYP61 > 3.0.CO;2-.

Feng, L., Li, B.B., 2018. Establishment of High Precision Terrain Model of Eroded Gully with UAV Oblique Aerial Photos and Ground Control Points. Trans. Chin. Soc. Agr. Eng. 34, 88–95. http://doi.org/10.11975/j.issn.1002-6819.2018.03.012. (In Chinese).

Finkner, S.C., Nearing, M.A., Foster, G.R., Gilley, J.E., 1989. A Simplified Equation for Modeling Sediment Transport Capacity. Trans. ASAE 32, 1545–1550. https://doi.org/10.1016/S0021-8634(89)80072-1.

Foroutan-pour, K., Dutilleul, P., Smith, D.L., 1999. Advances in the implementation of the box-counting method of fractal dimension estimation. Appl. Math. Comput. 105, 195–210. https://doi.org/10.1016/S0096-3003(98)10096-6.

Gatto, L.W., 2000. Soil freeze–thaw-induced changes to a simulated rill: potential impacts on soil erosion. Geomorphology 32, 147–160. https://doi.org/10.1016/S0169-555X(99)00092-6.

Gilley, J.E., Elliot, W.J., Laflen, J.M., Simanton, J.R., 1993. Critical shear stress and critical flow rates for initiation of rilling. J. Hydrol. 142, 251–271. https://doi.org/10.1016/0022-1694(93)90013-Y.

Giménez, R., Govers, G., 2002. Flow Detachment by Concentrated Flow on Smooth and Irregular Beds. Soil Sci. Soc. Am. J. 66, 1475–1483. https://doi.org/10.2136/sssaj2002.1475.

Gómez, J.A., Darboux, F., Nearing, M.A., 2003. Development and evolution of rill networks under simulated rainfall. Water Resour. Res. 39, 1148. https://doi.org/10.1029/2002WR001437.

Gong, J.G., Wang, W.L., Guo, J.Q., 2008. Ephemeral gully erosion experiment on hydrodynamics parameter of concentrated flow in hilly area of Loess Plateau. Sci. Soil Water Conserv. 6, 93–100. http://doi.org/10.16843/j.sswc.2008.01.017. (In Chinese).

Govers, G., 1985. Selectivity and transport capacity of thin flows in relation to rill erosion. CATENA 12, 35–49. https://doi.org/10.1016/S0341-8162(85)80003-5.

Govers, G., 1991. Rill erosion on arable land in Central Belgium: Rates, controls and predictability. CATENA 18, 133–155. https://doi.org/10.1016/0341-8162(91)90013-N.

Govers, G., 1992. Relationship between discharge, velocity and flow area for rills eroding loose, non-layered materials. Earth Surf. Process. Landf. 17, 515–528. https://doi.org/10.1002/esp.3290170510.

Govers, G., Everaert, W., Poesen, J., Rauws, G., De Ploey, J., Lautridou, J.P., 1990. A long flume study of the dynamic factors affecting the resistance of a loamy soil to concentrated flow erosion. Earth Surf. Process. Landf. 15, 313–328. https://doi.org/10.1002/esp.3290150403.

Govers, G., Giménez, R., Van Oost, K., 2007. Rill erosion: Exploring the relationship between experiments, modelling and field observations. Earth-Sci. Rev. 84, 87–102. https://doi.org/10.1016/j.earscirev.2007.06.001.

Govindaraju, R.S., Kavvas, M.L., 1992. Characterization of the rill geometry over straight hillslopes through spatial scales. J. Hydrol. 130, 339–365. https://doi.org/10.1016/0022-1694(92)90116-D.

Guo, M., Shi, H., Zhao, J., Liu, P., Welbourne, D., Lin, Q., 2016. Digital close range photogrammetry for the study of rill development at flume scale. CATENA 143, 265–274. https://doi.org/10.1016/j.catena.2016.03.036.

Guo, M., Yang, B., Wang, W., Chen, Z., Wang, W., Zhao, M., Kang, H., 2019. Distribution, morphology and influencing factors of rills under extreme rainfall conditions in main land uses on the Loess Plateau of China. Geomorphology 345, 106847. https://doi.org/10.1016/j.geomorph.2019.106847.

Hamed, Y., Albergel, J., Pépin, Y., Asseline, J., Nasri, S., Zante, P., Berndtsson, R., El-Niazy, M., Balah, M., 2002. Comparison between rainfall simulator erosion and observed reservoir sedimentation in an erosion-sensitive semiarid catchment. CATENA 50, 1–16. https://doi.org/10.1016/S0341-8162(02)00089-9.

Han, P., Ni, J.R., Hou, K.B., Miao, C.Y., Li, T.H., 2011. Numerical modeling of gravitational erosion in rill systems. Int. J. Sediment Res. 26, 403–415. https://doi.org/10.1016/S1001-6279(12)60001-8.

He, J.J., Gong, H.L., Li, X.J., Cai, Q.G., 2014. Effects of rill development on runoff and sediment yielding processes. Adv. Water Sci. 25, 90–97. http://doi.org/10.14042/j.cnki.32.1309.2014.01.021. (In Chinese).

He, J.J., Lv, Y., Gong, H.L., Cai, Q.G., 2013. Experimental study on rill erosion characteristics and its runoff and sediment yield process. J. Hydraul. Eng. 44, 398–405. http://doi.org/10.13243/j.cnki.slxb.2013.04.005. (In Chinese).

Hieke, F., Schmidt, J., 2013. The effect of soil bulk density on rill erosion - Results of experimental studies. Zeitschrift fur Geomorphologie 57, 245–266. https://doi.org/10.1127/0372-8854/2012/0091.

Huang, C.H., Laflen, J., Bradford, J., 1996. Evaluation of the Detachment-Transport Coupling Concept in the WEPP Rill Erosion Equation. Soil Sci. Soc. Am. J. 60, 734–739. https://doi.org/10.2136/sssaj1996.03615995006000030008x.

Jester, W., Klik, A., 2005. Soil surface roughness measurement—methods, applicability, and surface representation. CATENA 64, 174–192. https://doi.org/10.1016/j.catena.2005.08.005.

Jiang, F., Zhan, Z., Chen, J., Lin, J., Wang, M.K., Ge, H., Huang, Y., 2018. Rill erosion processes on a steep colluvial deposit slope under heavy rainfall in flume experiments with artificial rain. CATENA 169, 46–58. https://doi.org/10.1016/j.catena.2018.05.023.

Jiang, Y., Shi, H., Wen, Z., Guo, M., Zhao, J., Cao, X., Fan, Y., Zheng, C., 2020. The dynamic process of slope rill erosion analyzed with a digital close range photogrammetry observation system under laboratory conditions. Geomorphology 350, 106893. https://doi.org/10.1016/j.geomorph.2019.106893.

Jiang, Z.S., Wang, Z.Q., Liu, Z., 1996. Quantitative Study on Spatial Variation of Soil Erosion in a Small Watershed in the Loess Hilly Region. J. Soil Water Conserv. 1–9 (In Chinese).

Kimaro, D.N., Poesen, J., Msanya, B.M., Deckers, J.A., 2008. Magnitude of soil erosion on the northern slope of the Uluguru Mountains, Tanzania: Interrill and rill erosion. CATENA 75, 38–44. https://doi.org/10.1016/j.catena.2008.04.007.

Kinnell, P., 2001. Particle travel distances and bed and sediment compositions associated with rain-impacted flows. Earth Surf. Process. Landf. 26, 749–758. https://doi.org/10.1002/esp.221.

Kinnell, P., 2006. Simulations demonstrating interaction between coarse and fine sediment loads in rain-impacted flow. Earth Surf. Process. Landf. 31, 355–367. https://doi.org/10.1002/esp.1249.

Kinnell, P., 2009. The influence of raindrop induced saltation on particle size distributions in sediment discharged by rain-impacted flow on planar surfaces. CATENA 78, 2–11. https://doi.org/10.1016/j.catena.2009.01.008.

Kinnell, P., 2016. Comparison between the USLE, the USLE-M and replicate plots to model rainfall erosion on bare fallow areas. CATENA 145, 39–46. https://doi.org/10.1016/j.catena.2016.05.017.

Knapen, A., Poesen, J., 2009. Soil erosion resistance effects on rill and gully initiation points and dimensions. Earth Surf. Process. Landf. 35, 217–228. https://doi.org/10.1002/esp.1911.

Krenz, J., Kuhn, N.J., 2018. Assessing Badland Sediment Sources Using Unmanned Aerial Vehicles. In: Nadal-Romero, E., Martínez-Murillo, J.F., Kuhn, N.J. (Eds.), Badlands Dynamics in a Context of Global Change. Elsevier, pp. 255–276.

Lei, T.W., Nearing, M.A., Haghighi, K., Bralts, V.F., 1998. Rill erosion and morphological evolution: A simulation model. Water Resour. Res. 34, 3157–3168. https://doi.org/10.1029/98WR02162.

Li, T., Li, S., Liang, C., He, B., Bush, R.T., 2019. Erosion vulnerability of sandy clay loam soil in Southwest China: Modeling soil detachment capacity by flume simulation. CATENA 178, 90–99. https://doi.org/10.1016/j.catena.2019.03.008.

Li, Z.W., Zhang, G.H., Geng, R., Wang, H., 2015. Rill erodibility as influenced by soil and land use in a small watershed of the Loess Plateau. China. Biosyst. Eng. 129, 248–257. https://doi.org/10.1016/j.biosystemseng.2014.11.002.

Lima, R.L.P.D., Abrantes, J.R.C.B., Lima, J.L.M.P.D., Lima, M.I.P.D., 2015. Using thermal tracers to estimate flow velocities of shallow flows: laboratory and field experiments. J. Hydrol. Hydromechanics 63, 259–266. https://doi.org/10.1515/johh-2015-0028.

Liu, B.Y., Yang, Y., Lu, S.J., 2018. Discriminations on common soil erosion terms and their implications for soil and water conservation. Sci. Soil Water Conserv. 16, 9–16. http://doi.org/10.16843/j.sswc.2018.01.002. (In Chinese).

Liu, K., Ding, H., Tang, G., Na, J., Huang, X., Xue, Z., Yang, X., Li, F., Levy, J., Kainz, W., 2016. Detection of Catchment-Scale Gully-Affected Areas Using Unmanned Aerial Vehicle (UAV) on the Chinese Loess Plateau. Int. J. Geo-Inf. 5, 238. https://doi.org/10.3390/ijgi5120238.

Liu, P., Li, X.Y., Wang, W., 2007. Runoff flow velocity measurement system using photoelectric sensor and tracing method. Trans. Chin. Soc. Agr. Eng. 23, 116–120. https://doi.org/10.3321/j.issn:1002-6819.2007.05.021. (In Chinese).

Liu, Q.Q., An, Y., 2007. Three Basic Dynamics Processes of Soil Erosion. Sci. Technol. Rev. 25, 28–37. https://doi.org/10.3321/j.issn:1000-7857.2007.14.005. (In Chinese).

Lu, H., Prosser, I., Moran, C., Gallant, J., Priestley, G., Stevenson, J., 2003. Predicting sheetwash and rill erosion over the Australian continent. Aus. J. Soil Res. 41, 1037–1062. https://doi.org/10.1071/SR02157.

Luk, S.-H., Abrahams, A.D., Parsons, A.J., 1993. Sediment sources and sediment transport by rill flow and interrill flow on a semi-arid piedmont slope, southern Arizona. CATENA 20, 93–111. https://doi.org/10.1016/0341-8162(93)90031-J.

Mahmoodabadi, M., Ghadiri, H., Rose, C., Yu, B., Rafahi, H., Rouhipour, H., 2014. Evaluation of GUEST and WEPP with a new approach for the determination of sediment transport capacity. J. Hydrol. 513, 413–421. https://doi.org/10.1016/j.jhydrol.2014.03.060.

Mancilla, G.A., Chen, S., McCool, D.K., 2005. Rill density prediction and flow velocity distributions on agricultural areas in the Pacific Northwest. Soil Tillage Res. 84,

54–66. https://doi.org/10.1016/j.still.2004.10.002.
Merz, W., Bryan, R.B., 1993. Critical conditions for rill initiation on sandy loam Brunisols: laboratory and field experiments in southern Ontario, Canada. Geoderma 57, 357–385. https://doi.org/10.1016/0016-7061(93)90050-U.
Mirzaee, S., Ghorbani-Dashtaki, S., 2018. Deriving and evaluating hydraulics and detachment models of rill erosion for some calcareous soils. CATENA 164, 107–115. https://doi.org/10.1016/j.catena.2018.01.016.
Mirzaee, S., Ghorbani-Dashtaki, S., Kerry, R., 2020. Comparison of a spatial, spatial and hybrid methods for predicting inter-rill and rill soil sensitivity to erosion at the field scale. CATENA 188, 104439. https://doi.org/10.1016/j.catena.2019.104439.
Misra, R.K., Rose, C.W., 1996. Application and sensitivity analysis of process-based erosion model GUEST. Eur. J. Soil Sci. 47, 593–604.
Moore, I.D., Burch, G.J., 1986. Sediment Transport Capacity of Sheet and Rill Flow: Application of Unit Stream Power Theory. Water Resour. Res. 22, 1350–1360. https://doi.org/10.1029/wr022i008p01350.
Morgan, R.P.C., Quinton, J.N., Smith, R.E., Govers, G., 1998. The European Soil Erosion Model (EUROSEM): A dynamic approach for predicting sediment transport from fields and small catchments. Earth Surf. Process. Landf. 23, 527–544. https://doi.org/10.1002/(SICI)1096-9837(199806)23:63.0.CO;2-5.
Mujtaba, B., Lima, J.L.M.P.D., 2018. Laboratory testing of a new thermal tracer for infrared-based PTV technique for shallow overland flows. CATENA 169, 69–79. https://doi.org/10.1016/j.catena.2018.05.030.
Nearing, M.A., Darrell, N., Bulgakov, D.A., Larionov, G., West, L., Dontsova, K., 1997. Hydraulics and erosion in eroding rills. Water Resour. Res. 33, 865–876. https://doi.org/10.1029/97WR00013.
Nearing, M.A., Bradford, J.M., Parker, S.C., 1991. Soil Detachment by Shallow Flow at Low Slopes. Soil Sci. Soc. Am. J. 55, 339–344. https://doi.org/10.2136/sssaj1991.03615995005500020006x.
Nearing, M.A., Foster, G.R., Lane, L.J., Finkner, S.C., 1989. A Process-Based Soil Erosion Model for USDA-Water Erosion Prediction Project. Trans. ASAE 32, 1587–1593. https://doi.org/10.13031/2013.31195.
Ni, S.M., Feng, S.Y., Wang, J.G., Cai, C.F., 2018. Relationship between rill erosion morphology and hydraulic characteristics and sediment yield on artificial soils slope with different textures. Trans. Chin. Soc. Agr. Eng. 34, 149–156 (In Chinese).
Niu, Y., Gao, Z., Li, Y., Lou, Y., Zhang, S., Zhang, L., Du, J., Zhang, X., Luo, K., 2020. Characteristics of rill erosion in spoil heaps under simulated inflow: A field runoff plot experiment. Soil Tillage Res. 202, 104655. https://doi.org/10.1016/j.still.2020.104655.
Nouwakpo, S., Huang, C.-H., Bowling, L., Owens, P., 2010. Impact of Vertical Hydraulic Gradient on Rill Erodibility and Critical Shear Stress. Soil Sci. Soc. Am. J. 74, 1914–1921. https://doi.org/10.2136/sssaj2009.0096.
Owoputi, L.O., Stolte, W.J., 1995. Soil Detachment in the Physically Based Soil Erosion Process: A Review. Trans. ASAE 38, 1099–1110. https://doi.org/10.13031/2013.27927.
Peng, W.Y., Zhang, Z.D., Zhang, K.L., 2015. Hydrodynamic characteristics of rill flow on steep slopes. Hydrol. Process. 29, 3677–3686. https://doi.org/10.1002/hyp.10461.
Polyakov, V.O., Nearing, M.A., 2003. Sediment transport in rill flow under deposition and detachment conditions. CATENA 51, 33–43. https://doi.org/10.1016/S0341-8162(02)00090-5.
Qin, C., Wells, R.R., Momm, H.G., Xu, X., Wilson, G.V., Zheng, F., 2019a. Photogrammetric analysis tools for channel widening quantification under laboratory conditions. Soil Tillage Res. 191, 306–316. https://doi.org/10.1016/j.still.2019.04.002.
Qin, C., Zheng, F., Wilson, G.V., Zhang, X.J., Xu, X., 2019b. Apportioning contributions of individual rill erosion processes and their interactions on loessial hillslopes. CATENA 181, 104099. https://doi.org/10.1016/j.catena.2019.104099.
Qin, C., Zheng, F., Xu, X., He, X., 2016. Measurement and Characteristics of Rill Geometry and Flow Parameter Based on Photogrammetry. Trans. Chin. Soc. Agr. Machi. 47, 150–156. https://doi.org/10.6041/j.issn.1000-1298.2016.11.020. (In Chinese).
Qin, C., Zheng, F., Zhang, X.J., Xu, X., Liu, G., 2018. A simulation of rill bed incision processes in upland concentrated flows. CATENA 165, 310–319. https://doi.org/10.1016/j.catena.2018.02.013.
Ran, H., Deng, Q.C., Zhang, B., Liu, H., Wang, L., Luo, M.L., Qin, F.C., 2018. Morphology and influencing factors of rills in the steep slope in Yuanmou Dry-Hot Valley (SW China). CATENA 165, 54–62. https://doi.org/10.1016/j.catena.2018.01.017.
Rauws, G., Auzet, A.V., 1989. Laboratory experiments on the effects of simulated tractor wheelings on linear soil erosion. Soil Tillage Res. 13, 75–81. https://doi.org/10.1016/0167-1987(89)90039-1.
Rauws, G., Govers, G., 1988. Hydraulic and soil mechanical aspects of rill generation on agricultural soils. Eur. J. Soil Sci. 39, 111–124. https://doi.org/10.1111/j.1365-2389.1988.tb01199.x.
Rieke-Zapp, D.H., Nearing, M.A., 2005. Slope shape effects on erosion: A laboratory study. Soil Sci. Soc. Am. J. 69, 1463–1471. https://doi.org/10.2136/sssaj2005.0015.
Römkens, M.J.M., Helming, K., Prasad, S.N., 2002. Soil erosion under different rainfall intensities, surface roughness, and soil water regimes. CATENA 46, 103–123. https://doi.org/10.1016/S0341-8162(01)00161-8.
Shainberg, I., Laflen, J.M., Bradford, J.M., Norton, L.D., 1994. Hydraulic Flow and Water Quality Characteristics in Rill Erosion. Soil Sci. Soc. Am. J. 58, 1007. https://doi.org/10.2136/sssaj1994.03615995005800040002x.
Shen, H.O., Zheng, F.L., Wen, L.L., Han, Y., Hu, W., 2016. Impacts of rainfall intensity and slope gradient on rill erosion processes at loessial hillslope. Soil Tillage Res. 155, 429–436. https://doi.org/10.1016/j.still.2015.09.011.
Shen, H.O., Zheng, F.L., Wen, L.L., Lu, J., Han, Y., 2014. An experimental study on rill morphology at loess hillslope. Acta Ecol. Sin. 34, 5514–5521. https://doi.org/10.5846/stxb201309172298. (In Chinese).
Shen, H.O., Zheng, F.L., Wen, L.L., Lu, J., Jiang, Y.L., 2015. An experimental study of rill erosion and morphology. Geomorphology 231, 193–201. https://doi.org/10.1016/j.geomorph.2014.11.029.
Sheridan, G.J.A.C., So, H.B.A., Loch, R.J.B.D., Walker, C.M.A., 2000. Estimation of erosion model erodibility parameters from media properties. Soil Res. 38, 265–284. https://doi.org/10.1071/sr99041.
Slattery, M.C., Bryan, R.B., 1992. Hydraulic conditions for rill incision under simulated rainfall: A laboratory experiment. Earth Surf. Process. Landf. 17, 127–146. https://doi.org/10.1002/esp.3290170203.
Smith, D.D., Wischmeier, W.H., 1957. Factors affecting sheet and rill erosion. Trans. Am. Geophys. Union 38, 889–896. https://doi.org/10.1029/TR038i006p00889.
Stefano, C.D., Ferro, V., Pampalone, V., Sanzone, F., 2013. Field investigation of rill and ephemeral gully erosion in the Sparacia experimental area, South Italy. CATENA 101, 226–234. https://doi.org/10.1016/j.catena.2012.10.012.
Stefano, C.D., Nicosia, A., Palmeri, V., Pampalone, V., Ferro, V., 2020. Dye-tracer technique for rill flows by velocity profile measurements. CATENA 185, 104313. https://doi.org/10.1016/j.catena.2019.104313.
Tauro, F., Aureli, M., Porfiri, M., Grimaldi, S., 2010. Characterization of Buoyant Fluorescent Particles for Field Observations of Water Flows. Sensors 10, 11512–11529. https://doi.org/10.3390/s101211512.
Tauro, F., Porfiri, M., Grimaldi, S., 2016. Surface flow measurements from drones. J. Hydrol. 540, 240–245. https://doi.org/10.1016/j.jhydrol.2016.06.012.
Tayfur, G., 2007. Modelling sediment transport from bare rilled hillslopes by areally averaged transport equations. CATENA 70, 25–38. https://doi.org/10.1016/j.catena.2006.07.002.
Tian, P., Xu, X.Y., Pan, C.Z., Hsu, K.L., Yang, T.T., 2017. Impacts of rainfall and inflow on rill formation and erosion processes on steep hillslopes. J. Hydrol. 548, 24–39. https://doi.org/10.1016/j.jhydrol.2017.02.051.
Tisdall, J.M., Oades, J.M., 1982. Organic matter and water-stable aggregates in soils. J. Soil Sci. 32, 141–163. https://doi.org/10.1111/j.1365-2389.1982.tb01755.x.
Torri, D., Sfalanga, M., Chisci, G.M., 1987. Threshold Conditions for Incipient Rilling. CATENA Suppl. 8, 97–105. https://doi.org/10.1002/aheh.19870150617.
Valentin, C., Poesen, J., Li, Y., 2005. Gully erosion: Impacts, factors and control. CATENA 63, 132–153. https://doi.org/10.1016/j.catena.2005.06.001.
Vinci, A., Brigante, R., Todisco, F., Mannocchi, F., Radicioni, F., 2015. Measuring rill erosion by laser scanning. CATENA 124, 97–108. https://doi.org/10.1016/j.catena.2014.09.003.
Vinci, A., Todisco, F., Mannocchi, F., 2016. Calibration of manual measurements of rills using Terrestrial Laser Scanning. CATENA 140, 164–168. https://doi.org/10.1016/j.catena.2016.01.026.
Wagenbrenner, J.W., Robichaud, P.R., Elliot, W.J., 2010. Rill erosion in natural and disturbed forests: 2. Modeling Approaches. Water Resour. Res. 46, W10507. https://doi.org/10.1029/2009WR008315.
Wang, D.D., Wang, Z.L., Shen, N., Chen, H., 2016. Modeling soil detachment capacity by rill flow using hydraulic parameters. J. Hydrol. 535, 473–479. https://doi.org/10.1016/j.jhydrol.2016.02.013.
Wang, Y., Luo, J., Zheng, Z., Li, T., He, S., Zhang, X., Wang, Y., Liu, T., 2019. Assessing the contribution of the sediment content and hydraulics parameters to the soil detachment rate using a flume scouring experiment. CATENA 176, 315–323. https://doi.org/10.1016/j.catena.2019.01.024.
Wells, R.R., Momm, H.G., Bennett, S.J., Gesch, K.R., Dabney, S.M., Cruse, R., Wilson, G.V., 2016. A Measurement Method for Rill and Ephemeral Gully Erosion Assessments. Soil Sci. Soc. Am. J. 80. https://doi.org/10.2136/sssaj2015.09.0320.
Westoby, M.J., Brasington, J., Glasser, N.F., Hambrey, M.J., Reynolds, J.M., 2012. 'Structure-from-Motion' photogrammetry: A low-cost, effective tool for geoscience applications. Geomorphology 179, 300–314. https://doi.org/10.1016/j.geomorph.2012.08.021.
Wirtz, S., Seeger, M., Remke, A., Wengel, R., Wagner, J.-F., Ries, J.B., 2013. Do deterministic sediment detachment and transport equations adequately represent the process-interactions in eroding rills? An experimental field study. CATENA 101, 61–78. https://doi.org/10.1016/j.catena.2012.10.003.
Wirtz, S., Seeger, M., Ries, J.B., 2012. Field experiments for understanding and quantification of rill erosion processes. CATENA 91, 21–34. https://doi.org/10.1016/j.catena.2010.12.002.
Wu, B., Wang, Z.L., Shen, N., Wang, S., 2016. Modelling sediment transport capacity of rill flow for loess sediments on steep slopes. CATENA 147, 453–462. https://doi.org/10.1016/j.catena.2016.07.030.
Xiao, P.Q., Zheng, F.L., Wang, X.Y., Yao, W.Y., 2008. Experimental Study on Erosion Pattern Evolvement and Sediment Process on Loessal Hillslopes. J. Soil Water Conserv., 24–27. http://doi.org/10.13870/j.cnki.stbcxb.2008.01.024. (In Chinese).
Yan, L.J., Yu, X.X., Lei, T.W., Zhang, Q.W., Qu, L.Q., 2008. Effects of transport capacity and erodibility on rill erosion processes: A model study using the Finite Element method. Geoderma 146, 114–120. https://doi.org/10.1016/j.geoderma.2008.05.009.
Yang, C., Su, Z.A., Xiong, D.H., Yang, H.K., Xu, X., Dong, Y.F., 2018. Application of Close-range Photogrammetry Technology in the Study of Soil Erosion Rate on Slope Farmland. J. Soil Water Conserv. 32, 121-127 + 134. http://doi.org/10.13870/j.cnki.stbcxb.2018.01.020. (In Chinese).
Yang, C.T., 1972. Unit stream power and sediment transport. J. Hydraulic Division 98, 1805–1826. https://doi.org/10.1016/S0022-460X(74)80150-1.
Yang, D.M., Gao, P.L., Zhao, Y.D., Zhang, Y.H., Liu, X.Y., Zhang, Q.W., 2018b. Modeling sediment concentration of rill flow. J. Hydrol. 561, 286–294. https://doi.org/10.1016/j.jhydrol.2018.04.009.
Yanosek, K.A., Foltz, R.B., Dooley, J.H., 2006. Performance assessment of wood strand erosion control materials among varying slopes, soil textures, and cover amounts. J. Soil Water Conserv. 61, 45–51. https://doi.org/10.1016/j.geoderma.2005.02.023.
Yao, C., Lei, T., Elliot, W.J., McCool, D.K., Zhao, J., Chen, S., 2008. Critical Conditions for

Rill Initiation. Trans. ASABE 51, 107–114. https://doi.org/10.13031/2013.24231.
Yao, C., Lei, T., Zhang, Q., Zhao, J., Xiao, J., 2004. Theoretical Analysis of Errors in Rill Erodibility Parameter Estimation Used in WEPP Model. ASAE/CSAE Annual International Meeting, Ottawa, Canada.
Zhang, C.B., Yang, S.T., Zhao, C.S., Lou, H.Z., Zhang, Y.C., Bai, J., Wang, Z.W., Guan, Y.B., Zhang, Y., 2018. Topography Data Accuracy Vertification of Small Consumer UAV. J. Remote Sens. 22, 185–195. http://doi.org/10.11834/jrs.20186483. (In Chinese).
Zhang, F.B., Yang, M.Y., 2010. Plot-Slope Soil Erosion Using 7Be Measurement and Rill fractal Dimension. J. Nucl. Agr. Sci. 24, 1032–1037. https://doi.org/10.1016/S1876-3804(11)60004-9. (In Chinese).
Zhang, G.H., Liu, B.Y., Liu, G.B., He, X.W., Nearing, M.A., 2003. Detachment of Undisturbed Soil by Shallow Flow. Soil Sci. Soc. Am. J. 67, 713–719. https://doi.org/10.2136/sssaj2003.0713.
Zhang, G.H., Liu, Y.M., Han, Y.F., Zhang, X.C., 2009. Sediment Transport and Soil Detachment on Steep Slopes: I. Transport Capacity Estimation. Soil Sci. Soc. Am. J. 73, 1291–1297. https://doi.org/10.2136/sssaj2008.0145.
Zhang, G.H., Luo, R.T., Cao, Y., Shen, R.C., Zhang, X.C., 2010. Correction factor to dye-measured flow velocity under varying water and sediment discharges. J. Hydrol. 389, 205–213. https://doi.org/10.1016/j.jhydrol.2010.05.050.
Zhang, J., Zheng, F.L., Wen, L.L., Yu, F.Y., An, J., Li, G.F., 2011. Methodology of Dynamic Monitoring Gully Erosion Process Using 3D Laser Scanning Technology. Bull. Soil Water Conserv. 31, 89–94. http://doi.org/10.13961/j.cnki.stbctb.2011.06.034. (In Chinese).
Zhang, K.L., Yasuhiro, A., 1998. Critical Hydraulic Condition of Rill Erosion on Sloping Surface. J. Soil Water Conserv. 4, 42–47 (In Chinese).
Zhang, P., Tang, H.W., Yao, W.Y., Zhang, N., Lv, X.Z., 2016. Experimental investigation of morphological characteristics of rill evolution on loess slope. CATENA 137, 536–544. https://doi.org/10.1016/j.catena.2015.10.025.
Zhang, P., Yao, W.Y., Chen, W., 2014. Quantitative description of rill morphology on the rainfall-driven loess hillslope by fractal and entropy. Sci. Soil Water Conserv. 12, 17–22. http://doi.org/10.16843/j.sswc.2014.05.003. (In Chinese).
Zhang, P., Yao, W.Y., Liu, G.B., Xiao, P.Q., 2019. Experimental study on soil erosion prediction model of loess slope based on rill morphology. CATENA 173, 424–432. https://doi.org/10.1016/j.catena.2018.10.034.
Zhang, P., Zheng, F.L., Wang, B., Chen, J.Q., Ding, X.B., 2008. Comparative Study of Monitoring Gully Erosion Morphology Change Process by Using High Precision GPS, Leica HDS 3000 Laser Scanner and Needle Board Method. Bull. Soil Water Conserv. 28, 11-15 + 20. 10.13961/j.cnki.stbctb.2008.05.015. (In Chinese).
Zhang, X.C., Liu, G., Zheng, F.L., 2018b. Understanding erosion processes using rare earth element tracers in a preformed interrill-rill system. Sci. Total Environ. 625, 920–927. https://doi.org/10.1016/j.scitotenv.2017.12.345.
Zhao, C.H., Gao, J.E., 2016. Cross-section characteristics and hydraulic geometry of different erosion gullies on slopes. Adv. Water Sci. 27, 22–30. 10.14042/j.cnki.32.1309.2016.01.001. (In Chinese).
Zhao, L.S., Rui, H., Wu, F.Q., 2017. Effect of tillage on soil erosion before and after rill development. Land Degrad. Dev. 29, 2506–2513. https://doi.org/10.1002/ldr.2996.
Zheng, F.L., Zhang, X.C., Wang, J., Flanagan, D.C., 2020. Assessing applicability of the WEPP hillslope model to steep landscapes in the northern Loess Plateau of China. Soil Tillage Res. 197, 104492. https://doi.org/10.1016/j.still.2019.104492.
Zheng, F.L., Gao, X.T., 2003. Research Progresses in Hillslope Soil Erosion Processes. Geogr. Sci. 23, 230–235 (In Chinese).
Zheng, F.L., Yang, Q.K., Wang, Z.L., 2004. Water Erosion Prediction Model. Res. Soil Water Conserv. 13–24 (In Chinese).
Zhuang, X.H., Wang, W., Ma, Y.Y., Huang, X.F., Lei, T.W., 2018. Spatial distribution of sheet flow velocity along slope under simulated rainfall conditions. Geoderma 321, 1–7. https://doi.org/10.1016/j.geoderma.2018.01.036.